

See discussions, stats, and author profiles for this publication at: <https://www.researchgate.net/publication/261615121>

# Dry Synthesis of Easily Tunable Nano Ruthenium Supported on Graphene: Novel Nanocatalysts for Aerial Oxidation of Alcohols and Transfer Hydrogenation of Ketones

ARTICLE in THE JOURNAL OF PHYSICAL CHEMISTRY C · NOVEMBER 2013

Impact Factor: 4.77 · DOI: 10.1021/jp402978q

CITATIONS

26

READS

71

8 AUTHORS, INCLUDING:



**Gopiraman Mayakrishnan**

Shinshu University, Ueda, Japan

47 PUBLICATIONS 400 CITATIONS

SEE PROFILE



**Zeeshan Khatri**

Mehran University of Engineering and Technol...

30 PUBLICATIONS 198 CITATIONS

SEE PROFILE



**Ramasamy Karvembu**

National Institute of Technology Tiruchirappalli

156 PUBLICATIONS 1,678 CITATIONS

SEE PROFILE



**Ick-Soo Kim**

Shinshu University

195 PUBLICATIONS 1,684 CITATIONS

SEE PROFILE

# Dry Synthesis of Easily Tunable Nano Ruthenium Supported on Graphene: Novel Nanocatalysts for Aerial Oxidation of Alcohols and Transfer Hydrogenation of Ketones

Mayakrishnan Gopiraman,<sup>†</sup> Sundaram Ganesh Babu,<sup>‡</sup> Zeeshan Khatri,<sup>†</sup> Wei Kai,<sup>†</sup> Yoong Ahm Kim,<sup>⊥</sup> Morinobu Endo,<sup>§</sup> Ramasamy Karvembu,<sup>\*,‡</sup> and Ick Soo Kim<sup>\*,†</sup>

<sup>†</sup>Nano Fusion Technology Research Lab, Interdisciplinary Graduate School of Science and Technology, Shinshu University, Ueda, Nagano 386 8567, Japan

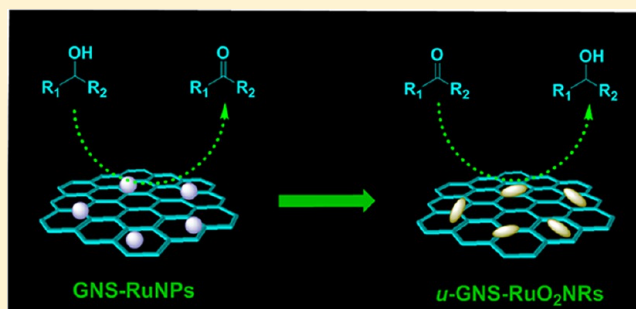
<sup>‡</sup>Department of Chemistry, National Institute of Technology, Tiruchirappalli 620 015, India

<sup>§</sup>Faculty of Engineering, Shinshu University, 4-17-1 Wakasato, Nagano-shi 380 8553, Japan

<sup>⊥</sup>Department of Polymer & Fiber System Engineering, Chonnam National University, 77 Yongbong-ro, buk-gu, Gwangju, 500-757, Korea

## S Supporting Information

**ABSTRACT:** In this study, ruthenium nanoparticles (RuNPs) were successfully decorated on graphene nanosheets (GNSs) for the very first time by a dry synthesis method. The resultant material (GNS-RuNPs) was used as a nanocatalyst for the aerial oxidation of alcohols after being optimized. The scope of the catalytic system was extended with various aliphatic, aromatic, alicyclic, benzylic, allylic, amino, and heterocyclic alcohols. The 0.036 mol % (5 mg) of catalyst was enough for aerial oxidation of alcohols, the lowest amount of catalyst so far reported. The proposed nanocatalyst is highly chemoselective, heterogeneous, and reusable. The GNS-RuNPs were separated out from the reaction mixture and analyzed by transmission electron microscopy (TEM), X-ray diffraction (XRD), Raman, and scanning electron microscopy-energy dispersive spectrometry (SEM-EDS); the results revealed that the nanocatalyst is physically as well as chemically stable. Owing to the high stability of used catalyst (*u*-GNS-RuNPs), it was further applied in transfer hydrogenation, after suitable modifications. We obtained ruthenium oxide nanorod hybrid GNSs (*u*-GNS-RuO<sub>2</sub>NRs) from *u*-GNS-RuNPs by simple calcination. The catalytic activity of *u*-GNS-RuO<sub>2</sub>NRs toward the transfer hydrogenation of various aromatic, alicyclic, and heterocyclic ketones was found to be excellent.



## 1. INTRODUCTION

Carbonyl compounds such as aldehydes and ketones serve as key and versatile intermediates in C–C bond-forming reactions and as a high-functional component in the perfume industry and are also used for the synthesis of fine chemicals.<sup>1–3</sup> To obtain these compounds via organic transformation, a selective oxidation of primary and secondary alcohols is the prime route.<sup>4–6</sup> Although several homogeneous and heterogeneous metal catalysts have been proposed,<sup>7–10</sup> particularly, metal nanoparticles (NPs) based on Pd,<sup>11</sup> Au,<sup>12</sup> Pt,<sup>13</sup> and Ru<sup>14</sup> play a tremendous role in the aerial oxidation process due to their high recyclability and easy separation from the reaction mixture. Among the numerous catalytic systems, the RuNP-based aerobic system is an effective, inexpensive, and extremely versatile synthetic tool to afford selectively oxygenated products.<sup>15–17</sup> Consequently, many RuNP-mediated aerial oxidation systems in mild reaction conditions such as low temperature and shorter reaction time have been devel-

oped.<sup>18–21</sup> In spite of the advantages, they often require higher stoichiometric amounts of Ru (typically 10–20 mol %), which lead to environmental hazard as well as less economical feasibility. Besides, high surface energies and strong van der Waals interactions in RuNPs promote unavoidable aggregation, and as a consequence, low catalytic activity as well as poor reusability were observed.<sup>11</sup> To control the aggregation of RuNPs, several inorganic and organic supports have been used, but their instability in high basic and acidic reaction conditions limits their use.<sup>22–24</sup> Owing to the better chemical stability and high surface area, activated carbon and CNTs have been used as a support for the active metal catalysts.<sup>25–29</sup> However, they too require higher stoichiometric amounts of Ru (typically 5.0–7.5 mol %), and the catalytic system has a very limited scope in

Received: March 26, 2013

Revised: October 8, 2013

Published: October 9, 2013

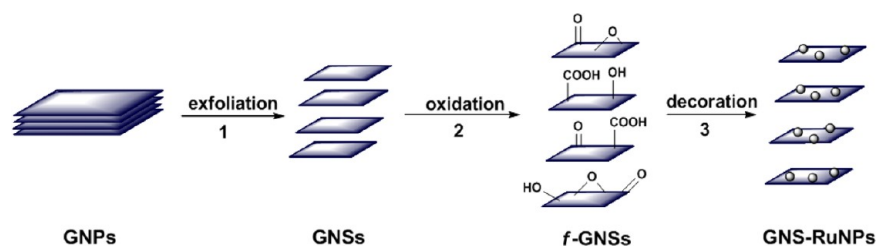


**Figure 1.** Schematic illustration for the preparation of GNS-RuNPs.

terms of yields and selectivity.<sup>30,31</sup> Therefore, developing an efficient, selective, stable, recyclable, and versatile catalyst for the aerial oxidation process with the use of a smaller amount of Ru remains a challenging task.

Very recently, graphene has been receiving greater attention owing to its astounding properties such as unique structure, high surface area, and chemical as well as electrochemical inertness.<sup>32–34</sup> Graphene plays a remarkable role as a support for transition metal NPs (MNPs) in the heterogeneous catalysis.<sup>35</sup> Particularly, graphene-supported transition MNPs demonstrated outstanding catalytic activities mainly due to the effective dispersion in various solvents, less aggregation of metal NPs, and larger surface area of the nanocatalysts.<sup>36</sup> Moreover, the decoration of MNPs onto the graphene support has shown more versatility in carrying out the highly selective catalytic processes.<sup>37</sup> Recently, Gil et al.<sup>38</sup> prepared PdNP-supported graphite oxide and used it as a catalyst for the Suzuki–Miyaura coupling reaction with higher activity than the commercial Pd–C catalyst. Kamat et al.<sup>39</sup> have investigated the interaction between graphene oxide and semiconductors (TiO<sub>2</sub>, ZnO), and graphene oxide and metal (Au, Pt) NPs. They have discussed their potential applications in catalysis, light–energy conversion, and fuel cells. We believe that the RuNPs based on graphene composite could overcome the above-discussed drawbacks especially higher stoichiometric amounts of Ru and the limited scope. In our study, RuNPs have been decorated over graphene nanosheets (GNS) by the dry synthesis method, and this was used as a nanocatalyst for the oxidation of alcohols. Chemoselectivity, heterogeneity, and reusability of the catalyst during the oxidation of alcohols were examined. The influence of the size of RuNPs on the oxidation of alcohols was also studied. Moreover, to investigate the versatility of the GNS-RuNPs, the used catalyst (*u*-GNS-RuNPs) was separated out from the reaction, converted into GNS-supported RuO<sub>2</sub> nanorods (*u*-GNS-RuO<sub>2</sub>NRs) by calcination, and used as a catalyst in the transfer hydrogenation of ketones. In fact, the reduction of ketones to their corresponding alcohols is also one of the essential organic transformations in both industrial and fine chemical processes.<sup>40</sup> Particularly,  $\alpha,\beta$ -unsaturated alcohols synthesized from this route have a high commercial value.<sup>41</sup> Hence the used catalyst was applied in the transfer hydrogenation of ketones after calcination.

## 2. EXPERIMENTAL SECTION

### 2.1. Dry Synthesis of Nanocatalyst (GNS-RuNPs).

Owing to the hydrophobic nature and chemical inertness of the graphene,<sup>42</sup> the decoration of metal NPs over graphene is a very difficult task. All previous studies so far reported used solution-based techniques, i.e., wet synthesis.<sup>43–45</sup> To obtain a homogeneous distribution and very good adhesion of metal NPs on graphene, many factors such as solvent, concentration

of metal precursor, reducing agent, deposition time, and temperature need to be controlled very carefully; therefore, a wet synthesis approach has limitations.<sup>46–48</sup> In contrast to wet synthesis, the solventless bulk synthesis, so-called “dry synthesis”, has been attracting greater interest due to its simplicity, better adhesion, and an advantage of the least parameters to be controlled.<sup>49</sup> Therefore, a straightforward dry synthesis method was adopted to decorate the RuNPs on GNSs. Initially, the bi- and few-layered graphene nanosheets (GNSs) were obtained from graphene nanoplatelets (GNPs) by a solution-phase exfoliation (SPE) method. In a typical procedure, 500 mL of *N*-methylpyrrolidone (NMP) containing 0.5 g of GNPs was sonicated for 12 h at 4 °C (step 1). The GNP-dispersed NMP solution was centrifuged and vacuum-dried. Then the resultant graphene nanosheets (GNSs, 0.5 g) were chemically treated with a 3:1 volume ratio mixture of concentrated H<sub>2</sub>SO<sub>4</sub> and HNO<sub>3</sub>. The mixture was sonicated at 40 °C for 3 h in an ultrasonic bath for the generation of functional groups (–COOH, –C=O, –C–O–C–, and –OH) on the GNS surface (step 2). After cooling to room temperature, the reaction mixture was diluted with 500 mL of deionized water and then vacuum-filtered through a filter paper of 3  $\mu$ m porosity. The resultant *f*-GNSs were repeatedly washed with deionized water until the pH reached neutral, and finally, the solid was vacuum-dried at 60 °C. After that, 0.13 g of Ru(acac)<sub>3</sub> was added into 0.5 g of *f*-GNS and mixed well by a mortar and pestle under ambient conditions. The homogeneous mixture of *f*-GNS and Ru(acac)<sub>3</sub> was obtained within 10–15 min. The impregnated Ru(acac)<sub>3</sub> was thermally decomposed into metallic RuNPs by calcination at 300 °C for 3 h under an argon atmosphere (step 3). Figure 1 shows a schematic illustration of the procedure for the preparation of GNS-RuNPs.

**2.2. Aerial Oxidation of Alcohols.** GNS-RuNPs (5 mg, 0.036 mol %) were stirred in 4 mL of toluene taken in a round-bottomed flask equipped with a condenser and a stirring bar. The substrate (1 mmol) was added to the stirring solution, and then the mixture was refluxed at 110 °C under atmospheric pressure of air. The oxidation reaction was monitored by thin-layer chromatography (TLC). After the completion of the reaction, the nanocatalyst was separated out from the reaction mixture by simple centrifugation, and the products and unconverted reactants were analyzed by GC. Selectivity of the product formed in each reaction was also calculated. Subsequently, the products of the selected oxidation reactions were isolated. The separated nanocatalyst was washed well with diethyl ether, dried at 130 °C for 3 h, and reused. The yield of the product, conversion, and selectivity were calculated by using eqs 1, 2, and 3, respectively.

$$\text{GC yield (\%)} = \% \text{ of product formed} \quad (1)$$



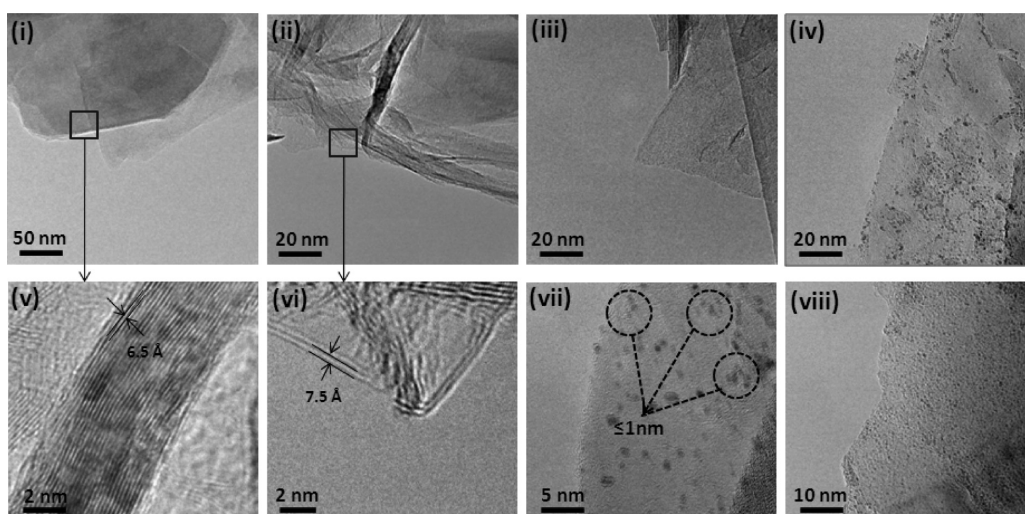


**Figure 2.** (i and v) TEM images of GNPs, (ii and vi) GNSs, (iii) *f*-GNSs, and (iv, vii, and viii) GNS-RuNPs.

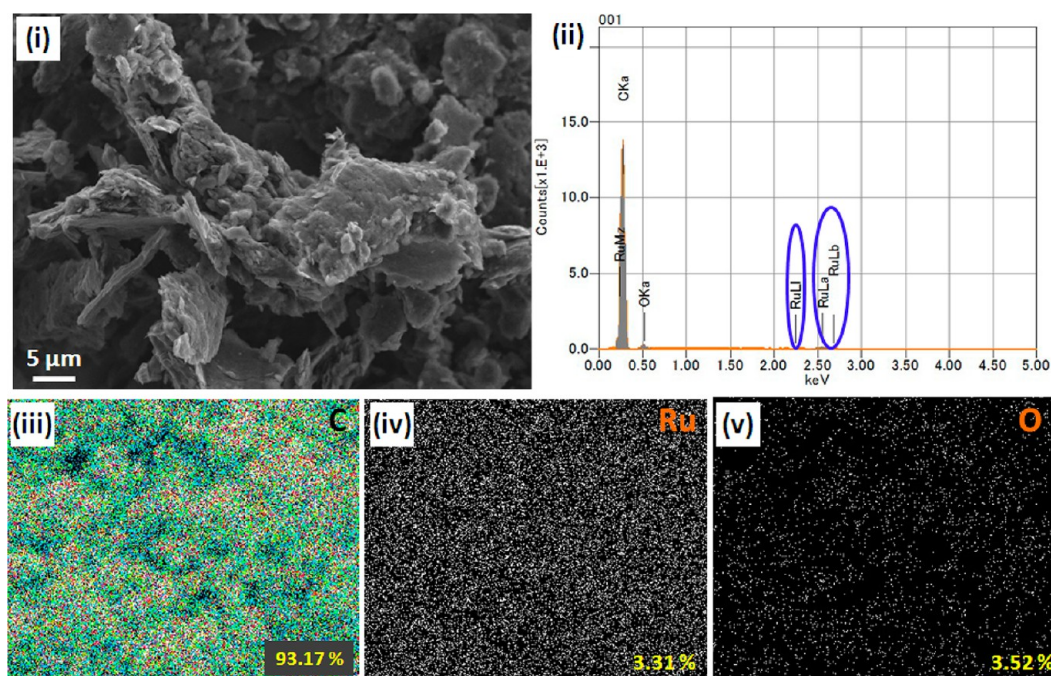


**Figure 3.** (i) SEM image and (ii) EDS spectra of GNS-RuNPs and corresponding elemental mapping observations of (iii) C, (iv) Ru, and (v) O.

$$\text{GC conversion (\%)} = 100 - \% \text{ of reactant remains} \quad (2)$$

$$\text{selectivity (\%)} = 100 - (\text{conversion} - \text{yield}) \quad (3)$$

**2.3. Transfer Hydrogenation of Ketones.** A mixture of *u*-GNS-RuO<sub>2</sub>NRs (5.0 mg, 0.033 mol % of Ru), substrate (1.0 mmol), 2-propanol (4 mL), and potassium *tert*-butoxide (112.21 mg, 1 mmol) was refluxed at 82 °C. The nanocatalyst was separated out from the reaction mixture after the completion of the reaction by simple centrifugation, and the products and unconverted reactants were analyzed by GC. Selectivity of the product was also calculated.

### 3. RESULTS AND DISCUSSION

**3.1. Characterization of GNS-RuNPs.** To investigate the morphology and fairly accurate number of GNS layers (bi- or few-layer), TEM images were taken for pure GNPs, GNS, *f*-GNS, and GNS-RuNPs (Figure 2). The TEM image [Figure

2(i)] showed that the GNPs were two-dimensional and pure. As seen from the magnified TEM images [Figure 2(i) and (v)], most of the GNPs were found as irregular ultrathin sheets having size ranging from 0.5 to 2 μm. Further, GNPs showed a multilayer with an average thickness of about 7–9 nm, whereas the GNPs after the SPE process with NMP [Figure 2(ii)] exhibited a continuous, wrinkled, and transparent sheet with an average thickness of about 0.8–2 nm, indicating the successful generation of GNSs.<sup>50</sup> To confirm the formation of GNSs, Brunauer–Emmett–Teller (BET) surface area was determined for GNPs and GNSs. It was found that the BET surface area of GNSs was obviously higher (103.1 m<sup>2</sup> g<sup>−1</sup>) than that of the GNPs (62.5 m<sup>2</sup> g<sup>−1</sup>). These results are consistent with one of our previous reports;<sup>51</sup> Raman, XRD, and XPS results also substantiate the existence of GNS (few) layers. For more details, refer to the TEM images in the Supporting Information (Figure S1). Ultrafine RuNPs were homogeneously dispersed

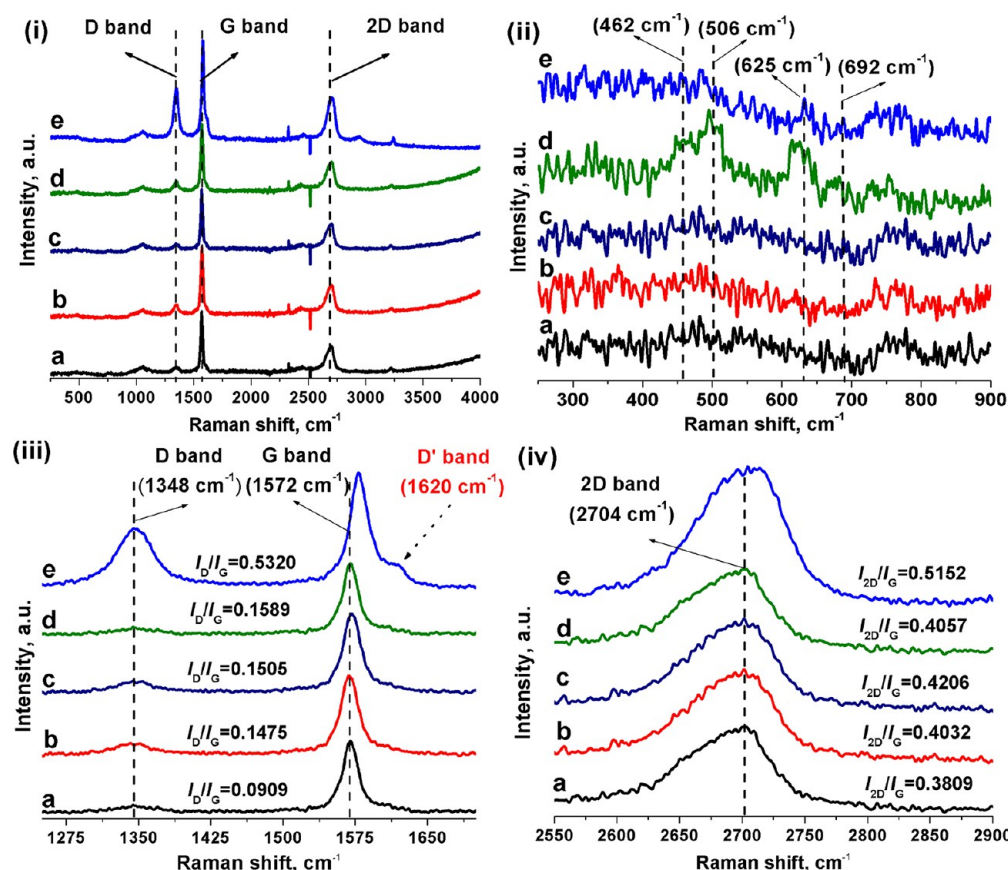


**Figure 4.** (i) Full and (ii, iii, and iv) magnified Raman spectra of (a) GNPs, (b) GNS, (c) *f*-GNS, (d) GNS + Ru(acac)<sub>3</sub>, and (e) GNS-RuNPs.

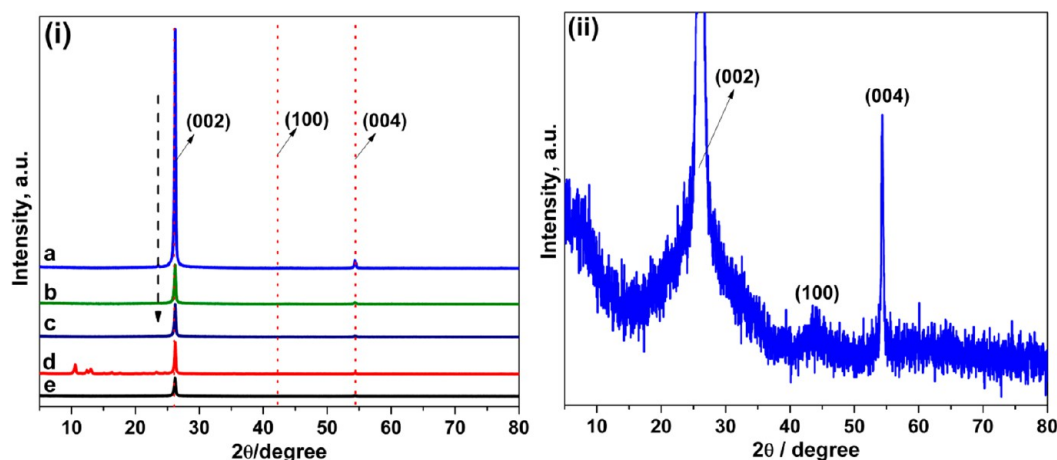
on the surface of GNSs [Figure 2(iv)]. The factual size of these attached RuNPs was found to be around 0.5–3.0 nm. Referring to the TEM images [Figure 2(vii) and (viii)], RuNPs were adhered on the anchoring sites of GNSs with a very narrow particle size distribution ranging from 0.5 to 3 nm. The mean diameter of RuNPs was found to be ca. 1.7 nm. Furthermore, no free RuNPs were found in the background of the TEM images [Figures 2(iv), (vii), and (viii)], which confirmed the complete utilization of RuNPs. The GNS-RuNPs have a BET surface area of 83.3 m<sup>2</sup> g<sup>−1</sup> with a pore volume of 0.392 cm<sup>3</sup> g<sup>−1</sup> and a BJH desorption average pore diameter of 19 nm. In addition, the surface area per unit mass (*S*) of RuNPs was calculated to be 283.42 m<sup>2</sup> g<sup>−1</sup> based on the equation  $S = 6000/(\rho \times d)$ , where *d* is the mean diameter of RuNPs (1.7 nm) and  $\rho$  is the density of Ru (12.45 g cm<sup>−3</sup>).<sup>52</sup>

Figure 3 shows the SEM-EDS and their corresponding elemental mapping images of GNS-RuNPs. The weight percentage of Ru in GNS-RuNPs was 3.31, as determined by EDS analysis [Figure 3(ii)]. From Figure 3(v), the weight percentage of oxygen was found to be 3.52 which indicates the presence of −OH groups in GNS-RuNPs. Figures 3(iv) and 3(v) depict the homogeneous distribution of RuNPs in GNS-RuNPs. The credibility of the proposed method can be recognized from the purity of GNS-RuNPs that contain only carbon, ruthenium, and oxygen elements as confirmed by EDS analysis (Figure 3).

Raman spectra were recorded for GNPs (a), GNSs (b), *f*-GNSs (c), GNS-Ru(acac)<sub>3</sub> [Ru(acac)<sub>3</sub> and GNS mixture before calcination] (d), and GNS-RuNPs (e), under 514.5 nm excitation over the Raman shift interval of 250–4000 cm<sup>−1</sup> (Figure 4). It is well known that graphene shows Raman

features in the region 800–2000 cm<sup>−1</sup>.<sup>53</sup> As expected, all five samples (a–e) exhibited three main Raman features, corresponding to the well-defined D-band line at ~1345 cm<sup>−1</sup>, G-band line at ~1570 cm<sup>−1</sup>, and 2D-band line at ~2700 cm<sup>−1</sup>.<sup>54</sup> The G-band line was originated from the in-plane vibration of sp<sup>2</sup> carbon atoms, which represented the relative degree of graphitization.<sup>55</sup> The D-band line was related to the amount of disorder which arises only in the presence of defects, indicating the presence of sp<sup>3</sup> carbon atoms or defect sites in graphene.<sup>56</sup> The 2D band line at 2700 cm<sup>−1</sup> is an overtone of the D band. Obviously, the intensity ratios of D, G, and 2D bands ( $I_D/I_G$  and  $I_{2D}/I_G$ ) are often used as a diagnostic tool to evaluate the number of layers and defect concentration in graphene.<sup>57</sup> The calculated intensity ratios for all five samples are shown in Figures 4(iii) and (iv). The  $I_D/I_G$  (0.1475) and  $I_{2D}/I_G$  (0.4032) values of GNSs were found to be higher than the  $I_D/I_G$  (0.0909) and  $I_{2D}/I_G$  (0.3809) of GNPs, which indicated the effective exfoliation of GNPs. Besides, the shape of the 2D band [Figure 4(iv)] was also significantly changed.<sup>51</sup> These changes confirmed the successful generation of bi- and few-layered GNSs, and as a consequence, the surface area has been increased.<sup>51</sup> Figure 4(iii) confirms the chemical functionalization of the GNS surface by −COOH, −C≡O, −C−O−C−, and −OH groups as the  $I_D/I_G$  (0.1505) and  $I_{2D}/I_G$  (0.4206) ratios were high for *f*-GNS when compared to that of pure GNS ( $I_D/I_G = 0.0909$  and  $I_{2D}/I_G = 0.3809$ ). Indeed, these functional groups act as effective nucleation centers for RuNPs, which assist homogeneous decoration as well as better adhesion of RuNPs on the GNS.<sup>58</sup> It is noteworthy that the  $I_D/I_G$  (0.5320) ratio of sample e was about four times higher than that of *f*-GNS (c), and in comparison to the *f*-GNS (c), a





**Figure 5.** (i) XRD pattern of (a) GNPs, (b) GNSs, (c) *f*-GNSs, (d) GNS + Ru(acac)<sub>3</sub>, and (e) GNS-RuNPs and (ii) magnified XRD pattern of GNS-RuNPs.

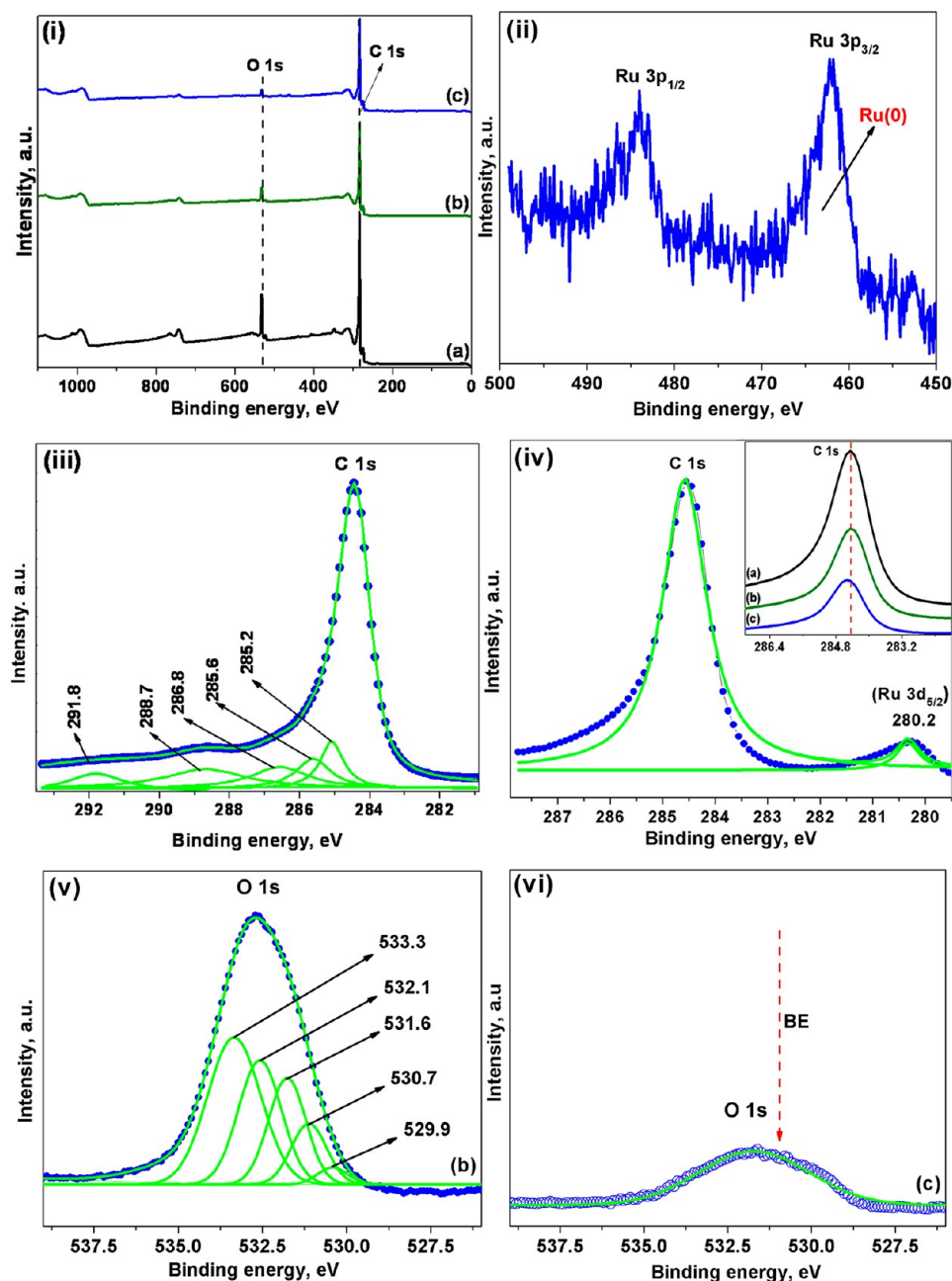
positive shift in G band (1570 to 1578 cm<sup>-1</sup>) was observed in **e**, which confirmed the attachment of RuNPs on the surface of GNSs. Apart from these relative intensity ratios, the Raman spectrum of sample **d** showed four new peaks at 462, 506, 625, and 692 cm<sup>-1</sup> [Figure 4(ii)], which are attributed to the presence of acetylacetonate groups. However, these peaks completely disappeared in sample **e** which revealed that Ru(acac)<sub>3</sub> was converted into metallic Ru.<sup>59</sup> Furthermore, the presence of a shoulder peak at 1620 cm<sup>-1</sup> in sample **e** indicated the presence of larger defect sites in GNSs; this may be due to a very strong attachment of RuNPs and/or may be caused by further fragmentation of GNSs into smaller sheets during the preparation process.<sup>60</sup>

Figure 5 shows XRD patterns of pure GNPs (**a**), GNSs (**b**), *f*-GNSs (**c**), GNS-Ru(acac)<sub>3</sub> (**d**), and GNS-RuNPs (**e**). All five samples (**a–e**) showed diffraction peaks at 26.5°, 44.2°, and 54.8°, corresponding to the (002), (100), and (004) crystal planes of graphite, respectively, which are attributed to the hexagonal graphite structures of GNSs.<sup>61</sup> As a result of the SPE process, a significant decrease in the intensity of the diffraction peak at 26.5° was observed in **b** compared to **a**, which confirmed the generation of layered GNSs [Figure 5(i)].<sup>62,63</sup> A further decrease in the intensity of this peak in sample **c** might be due to the presence of functional groups in *f*-GNSs. In fact, the interlayers of carbon stacked by van der Waals forces have interaction energy of about 2 eV/nm<sup>2</sup>.<sup>64</sup> To break this energy, typically a ~300 nN/lm<sup>2</sup> magnitude of force is required.<sup>64</sup> This extremely weak force might be achieved during the mixing/grinding process. The sample **d** exhibited a typical XRD pattern for acetylacetonate groups of Ru(acac)<sub>3</sub> (JCPDS No. 14-0733), whereas the sample **e** showed no diffraction peaks for Ru (Figure 3), which implied that Ru particles were of nanocrystalline nature.<sup>65</sup> Moreover, the absence of acetylacetonate peaks at around 12.0° in the sample **e** confirmed that Ru(acac)<sub>3</sub> was completely converted into Ru on the surface of GNSs.

To investigate the functionalization on GNSs and the chemical state of Ru in GNS-RuNPs, XPS spectra were recorded for GNSs, *f*-GNSs, and GNS-RuNPs; the results are shown in Figure 6. As expected, all three samples showed a C 1s peak and a O 1s peak at 284.6 and 532.8 eV, respectively [Figure 6(i)]. To find the shift in the peak, curve fitting was performed on C 1s and O 1s spectra of *f*-GNS and GNS-RuNPs using a Gaussian–Lorentzian peak shape. Prior to peak fitting, a Shirley baseline correction was done. The binding

energy (BE) of the C–C and C–H bonds were assigned at 284.5–285 eV, and the peaks at 285.2, 285.6, 286.8, and 288.7 eV were ascribed to C–OH, –C–O–C–, C=O, and –COOH groups, respectively [Figure 6(iii)].<sup>66</sup> Similarly, deconvolution of the O 1s spectra of *f*-GNS [Figure 6(v)] resulted in five peaks located at 529.9, 530.7, 531.6, 532.1, and 533.3 eV, which were assigned to the C=O, –COOH, C–OH, –C–O–C–, and H<sub>2</sub>O, respectively.<sup>66</sup> In comparison to the C 1s spectrum of GNS [Figure S2 (i) in Supporting Information], the intensity of the  $\pi \rightarrow \pi^*$  shakeup satellite peak at 291.5 eV significantly decreased, which supports the successful functionalization of GNSs.<sup>67</sup> In fact, the presence of carboxylic groups makes GNS hydrophilic and assists homogeneous decoration and good adhesion of RuNPs.<sup>68</sup> Mainly, the –COOH group plays a bridging role between the RuNPs and GNSs by exchanging the proton of the carboxyl group of the *f*-GNS with RuNPs; hence, a strong attachment of RuNPs on the surface of GNSs was achieved.<sup>68</sup> The XPS spectrum of the GNS-RuNPs in the Ru 3p region [Figure 6(ii)] showed BE for Ru 3p<sub>3/2</sub> at 461.0 eV and Ru 3p<sub>1/2</sub> at 483.2 eV, which corresponds to the photoemission from metallic Ru.<sup>69</sup> In Figure 6(vi), GNS-RuNPs showed a Ru 3d<sub>5/2</sub> peak at 280.2 eV which was attributed to the metallic Ru.<sup>69</sup> The overlapping of the C 1s and the Ru 3d<sub>3/2</sub> peaks at ~285 eV made it difficult to assign the BE of Ru 3d<sub>3/2</sub>. Referring to the O 1s spectrum of GNS-RuNPs [Figure 6(vi)], all the deconvoluted peaks (529.9, 530.7, 532.1, and 533.3 eV) disappeared except the weak one related to the C–OH bond (~531.6 eV) as compared with the O 1s spectrum of *f*-GNS [Figure 6(v)]. Alike, in the C 1s spectrum of GNS-RuNPs [Figure S2 (ii) in Supporting Information], the deconvoluted peaks at the binding energies of 285.6, 286.8, and 288.7 eV completely disappeared. The disappearance of the deconvoluted peaks in both O 1s and C 1s spectra of GNS-RuNPs showed a virtually complete reduction of the oxygen functional groups (C=O, –COOH, and –C–O–C–).<sup>66</sup> Interestingly, a positive shift in C 1s peak was observed for GNS-RuNPs when compared with that of the *f*-GNS; this confirmed the strong interaction between GNSs and RuNPs.<sup>70</sup> Furthermore, the decrease in the intensity of the C 1s peak in GNS-RuNPs in comparison to GNSs is an indication of generation of few-layered GNSs.<sup>71</sup> These results are in well agreement with the results of TEM, Raman, and XRD.

**3.2. Optimization of Reaction Conditions for the Oxidation of Alcohols.** To find the optimum reaction

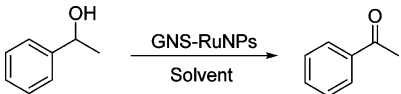


**Figure 6.** (i) XPS spectra of (a) GNSs, (b) *f*-GNSs and (c) GNS-RuNPs, (ii) main peaks of Ru 3p of GNS-RuNPs, (iii) C 1s peak of *f*-GNSs, (iv) main peaks of Ru 3d and O 1s of GNS-RuNPs [insert: C 1s peak of (a), (b) and (c)], and (v and vi) magnified O 1s peak of *f*-GNS and GNS-RuNPs.

conditions for the oxidation of alcohols, we used 1-phenylethanol as a substrate, and results are given in Table 1. Various organic solvents such as *N,N*-dimethylacetamide (DMAc), *N,N*-dimethylformamide, toluene, and dimethyl sulfoxide (DMSO) were tested in the oxidation reaction (Table 1, entries 1–4). The high yield of 99% was achieved when the reaction was carried out in toluene. As expected, no oxidized product was obtained in the absence of GNS-RuNPs (Table 1, entry 5). The optimum amount of GNS-RuNP catalyst was found to be 5 mg (0.036 mol %) (Table 1, entries 3 and 6–8). To the best of our knowledge, this is the lowest amount of Ru catalyst reported for the aerial oxidation of alcohols to date. In temperature optimization, a maximum yield of 99% was obtained when the reaction was stirred at 110 °C (Table 1,

entries 3 and 9–11). The reaction time of 16 h was found to be an optimum (Table 1, entries 3 and 12–21). Finally, to confirm the reaction to be aerobic, the reaction was performed under N<sub>2</sub> atmosphere using the optimized reaction conditions. A very low conversion (13%) was observed under N<sub>2</sub> atmosphere; this confirmed that GNS-RuNPs oxidize the alcohols using atmospheric O<sub>2</sub>.

**3.3. Extension of Scope.** The optimized reaction conditions were applied to the oxidation of various aliphatic, aromatic, alicyclic, benzylic, allylic, amino, and heterocyclic alcohols (Table 2). Results in Table 2 revealed that a variety of alcohols could be oxidized into their corresponding carbonyl compounds in good to excellent yields with high selectivity. Active aryl secondary alcohol, 1-phenylethanol, was oxidized to

**Table 1. Optimization of the Reaction Conditions for Oxidation of 1-Phenylethanol<sup>a</sup>**


entry	solvent <sup>b</sup>	amount of catalyst (mol %)	temperature (°C)	time (h)	yield <sup>c</sup> (%)
1	DMAc	0.036	110	16	48
2	DMF	0.036	110	16	35
3	<b>Toluene</b>	<b>0.036</b>	<b>110</b>	<b>16</b>	<b>99</b>
4	DMSO	0.036	110	16	61
5	Toluene	0	110	16	0
6	Toluene	0.018	110	16	14
7	Toluene	0.054	110	16	99
8	Toluene	0.072	110	16	99
9	Toluene	0.036	25	16	2
10	Toluene	0.036	50	16	14
11	Toluene	0.036	80	16	91
12	Toluene	0.036	110	0	0
13	Toluene	0.036	110	2	3
14	Toluene	0.036	110	4	4
15	Toluene	0.036	110	6	5
16	Toluene	0.036	110	8	5
17	Toluene	0.036	110	10	15
18	Toluene	0.036	110	12	17
19	Toluene	0.036	110	14	18
20	Toluene	0.036	110	18	99
21	Toluene	0.036	110	20	99

<sup>a</sup>All the reactions were performed with 1.0 mmol (117.0  $\mu$ L) of 1-phenylethanol. <sup>b</sup>4 mL of solvent was used in all the reactions. <sup>c</sup>GC yield.

acetophenone quantitatively with an excellent selectivity of 100% (Table 2, entry 1), whereas the Ru/CNT catalytic system gave only 64% of acetophenone.<sup>31</sup> Generally, the substrates with electron-donating substituents such as methoxy, bromo, or chloro are less reactive due to the mesomeric effect and, therefore, often exhibit lower yields.<sup>72</sup> However, in the present case, 1-phenylethanol containing an electron-donating substituent such as methoxy or chloro at the *para* position was effectively oxidized to the corresponding ketone in good yield without affecting the selectivity (Table 2, entries 2 and 3). In contrast to CrO<sub>3</sub>/H<sub>5</sub>IO<sub>6</sub> oxidation,<sup>73</sup> the 2-naphthyl ethanol was oxidized to 2-acetylnaphthalene in good yield (98%) without oxidizing the naphthalene ring (Table 2, entry 4). It was found that 1-phenyl-2-propanol was transformed to its corresponding ketone in moderate yield of 59% with 100% selectivity (Table 2, entry 5). In the conversion of diphenylcarbinol to benzophenone (Table 2, entry 6), the present catalytic system produced a better yield of 83% in comparison to the 28.2% yield of the Pd/C system.<sup>74</sup> Diphenylcarbinol with a chloro group at the *para* position also gave its corresponding ketone in excellent yield (93%) and selectivity (100%) (Table 2, entry 7). In the same way, 1-indanol was converted into 1-indanone in 86% yield after 22 h (Table 2, entry 8). The present catalytic system is also competent to oxidize the primary benzylic alcohols to the corresponding aldehydes effectively. Referring to entry 9 in Table 2, benzyl alcohol yielded benzaldehyde in excellent yield (95%) and selectivity (100%) without over-oxidation to benzoic acid, whereas the Ru-substituted silicotungstate catalytic system gave a poor yield of 64% with an overoxidation of benzyl alcohol to benzoic acid.<sup>75</sup> For the

transformation of 4-nitrobenzyl alcohol to 4-nitrobenzaldehyde (Table 2, entry 10), the present GNS-RuNP catalyst was very effective (95% yield after 24 h) compared to V<sub>2</sub>O<sub>5</sub> which gave only 79% of the desired product after 25 h.<sup>76</sup> Moreover, inspection of entry 11 in Table 2 revealed that cinnamyl alcohol yielded cinnamaldehyde in good yield of 81% (100% selectivity) without intramolecular hydrogen transfer or geometrical isomerization of the double bond.

Several existing Ru-based oxidation systems mainly suffer from the overoxidation of allylic and aliphatic alcohols to their corresponding carboxylic acids, which leads to lower selectivity and therefore hinders its industrial applications. It is worth mentioning that the present catalytic system showed a high selectivity (100%) toward the oxidation of allylic and aliphatic alcohols (Table 2, entries 12–15) without overoxidation. Allylic and aliphatic alcohols such as 2-propenol and 1-butanol were converted into the corresponding aldehydes in good to excellent yields (Table 2, entries 12 and 13). Less reactive 1-octanol was transformed into 1-octanone in good yield of 93% (Table 2, entry 14) without any overoxidation, whereas Ru-substituted silicotungstate-catalyzed oxidation of the same substrate gave only 14% of 1-octanone even after stirring for 48 h.<sup>75</sup> In the conversion of 2-octanol to 2-octanone (Table 2, entry 15), the present catalytic system gave a better yield of 56% (100% selectivity), whereas hydroxyapatite-supported palladium (PdHAP)-catalyzed oxidation yielded only 10.5% of 2-octanone.<sup>77</sup>

Less reactive cyclopentanol was converted into cyclopentanone in moderate yield of 60%, whereas the Au/Fe<sub>3</sub>O<sub>4</sub>@SiO<sub>2</sub> system produced only 42% yield (Table 2, entry 16).<sup>78</sup> A moderate yield (43%) of ketone was obtained from the oxidation of 1-cyclohexylethanol after stirring for 24 h (Table 2, entry 17). More interestingly, the sterically hindered alcohols such as 2-amino-2-methylpropan-1-ol and DL-isoborneol (Table 2, entries 18 and 19) were efficiently oxidized to their corresponding ketones. In spite of possessing a heterocyclic ring, 2-furyl ethanol (Table 2, entry 20) is capable of being oxidized to 2-acetyl furan in moderate yield (49%) in the present catalytic system.

Under the optimized reaction conditions, the active ruthenium oxo-species forms on the surface of GNSs. Obviously, the active species is unstable, and its formation is faster, which favors higher activity of the present catalytic system. The formation of ruthenium oxo-species was confirmed by XPS, Raman, and FT-IR (see Figure S3 in Supporting Information), which has been discussed in Section 3.8 (proposed mechanism). In addition to the role played by ruthenium oxo-species, the excellent catalytic activity of GNS-RuNPs is due to the three most important reasons: (i) the smaller size of the RuNPs, (ii) higher surface area of the GNS-RuNPs, and (iii) an effective dispersion of the GNS-RuNPs in the reaction medium.

**3.4. Chemoselective Nature of GNS-RuNPs.** To examine the chemoselectivity of the GNS-RuNPs, a series of reactions were carried out (Scheme 1). The present catalytic system can selectively oxidize the primary alcohol (benzyl alcohol or 1-octanol) in the presence of secondary alcohol (1-phenylethanol or 2-octanol). Oxidation of benzyl alcohol was faster compared to 1-octanol. Among 1-phenylethanol and 2-octanol, 1-phenylethanol undergoes oxidation faster. On the contrary, 1-phenylethanol was chemoselectively oxidized to obtain acetophenone in the presence of 1-octanol. This may be due



Table 2. Oxidation of Alcohols<sup>a</sup>

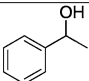
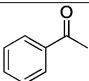
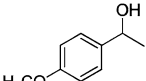
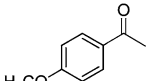
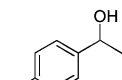
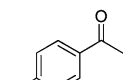
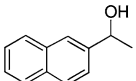
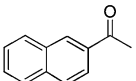
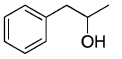
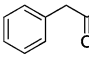
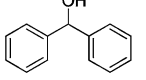
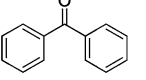
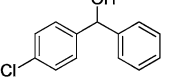
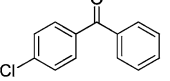
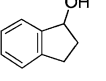
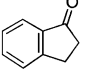
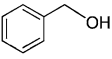
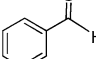
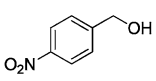
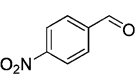
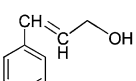
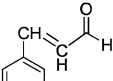
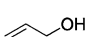
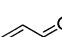
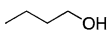
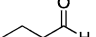
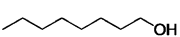
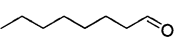
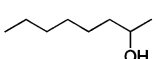
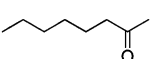
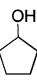
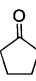
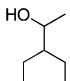
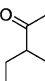
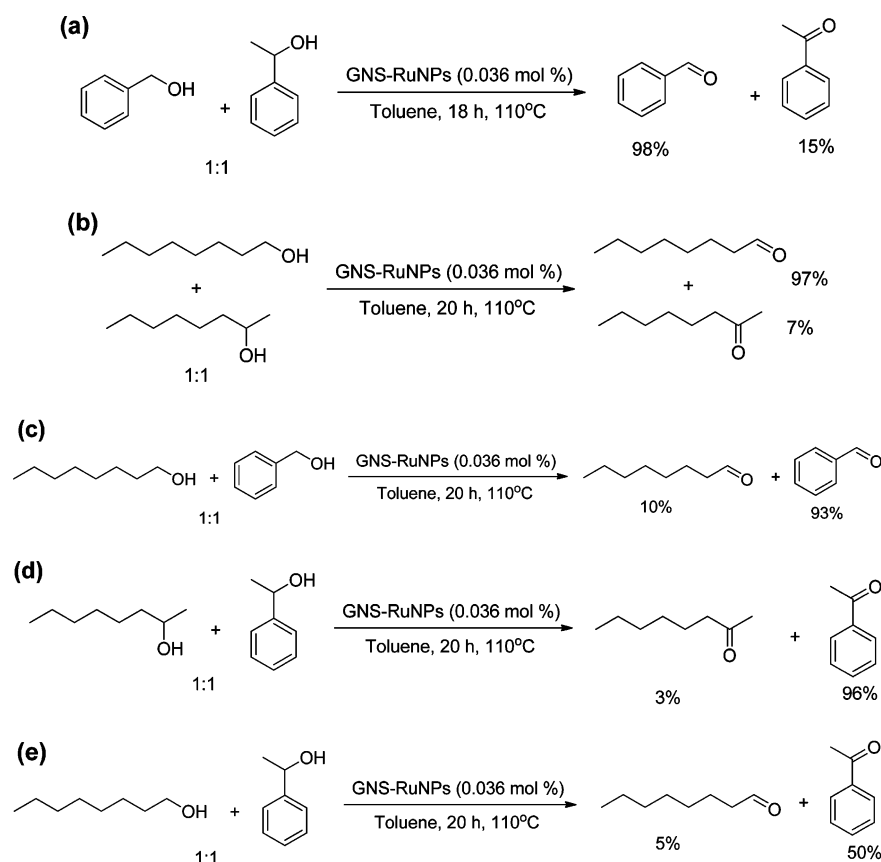
$\text{R}_1\text{CH(OH)R}_2 \xrightarrow[\text{Toulene, 110}^\circ\text{C}]{\text{GNS-RuNPs (0.036 mol\%)}} \text{R}_1\text{C(=O)R}_2$						
entry	substrate	product	t (h)	conv. <sup>b</sup> (%)	sel. <sup>b</sup> (%)	yield <sup>b</sup> (%)
1			16	99	100	99
2			16	86	100	86 (80) <sup>c</sup>
3			24	90	88	78
4			18	98	100	98 (95) <sup>c</sup>
5			18	59	100	59
6			20	83	100	83(79) <sup>c</sup>
7			22	93	100	93(86) <sup>c</sup>
8			22	86	77	63
9			18	95	100	95 (89) <sup>c</sup>
10			24	99	96	95 (93) <sup>c</sup>
11			21	81	100	81
12			9	67	100	67
13			22	93	100	93
14			20	93	100	93
15			20	56	100	56
16			24	63	94	60
17			22	70	73	43

Table 2. continued

entry	substrate	product	t (h)	conv. <sup>b</sup> (%)	sel. <sup>b</sup> (%)	yield <sup>b</sup> (%)
18			19	100	61	61
19			22	89	76	65
20			22	76	73	49

<sup>a</sup>Reaction conditions: substrate (1 equiv), GNS-RuNPs (0.036 mol %), toluene (4 mL), 110 °C. <sup>b</sup>Determined by GC analysis. <sup>c</sup>Isolated yield is given in paranthesis.

Scheme 1. Chemoselectivity of Nanocatalyst, GNS-RuNPs



to the better reactivity of 1-phenylethanol when compared to 1-octanol.

**3.5. Heterogeneity of GNS-RuNPs.** To inspect the factual heterogeneity of the GNS-RuNPs, a hot filtration test was performed for the oxidation of 1-phenylethanol under optimized reaction conditions. The nanocatalyst was separated out from the reaction mixture by a simple centrifugation after 8 h, and the yield of acetophenone determined by GC was 5%. Then the filtrate continued to be stirred for another 8 h, and the reaction conversion was monitored at 2 h intervals; the results are shown in Figure 7. It was noticed that there was no further conversion occurring after the GNS-RuNPs were separated out; this showed that the oxidation of 1-phenylethanol occurred only in the presence of GNS-RuNPs. In addition, the conversion remained 5% even after 16 h of the reaction time, which confirmed that the Ru was not leached out from GNS-RuNPs during the oxidation reaction. The filtrate

was further analyzed by ICP-MS; a trace amount of Ru content (9.8 ppb) confirmed the heterogeneous nature of the present catalytic system.

**3.6. Reusability of GNS-RuNPs.** Indeed, recovery and reusability are the important advantages of nanocatalysts, which make them economically feasible. GNS-RuNPs were separated out from the reaction mixture, washed with diethyl ether, and dried in vacuo at 130 °C. Then the recovered catalyst was reused for the oxidation of 1-phenylethanol; the results are presented in Figure 7. It is noteworthy that the present catalytic system provided 87% of acetophenone even at the fourth cycle, which confirmed its excellent reusability. Additionally, used nanocatalyst (*u*-GNS-RuNPs) was characterized by TEM, Raman, XRD, and SEM-EDS. The TEM images showed that the morphology of *u*-GNS-RuNPs remains unchanged [Figure S3(i) in Supporting Information]. SEM-EDS result revealed that the weight percentage of Ru in *u*-GNS-RuNPs was 3.01

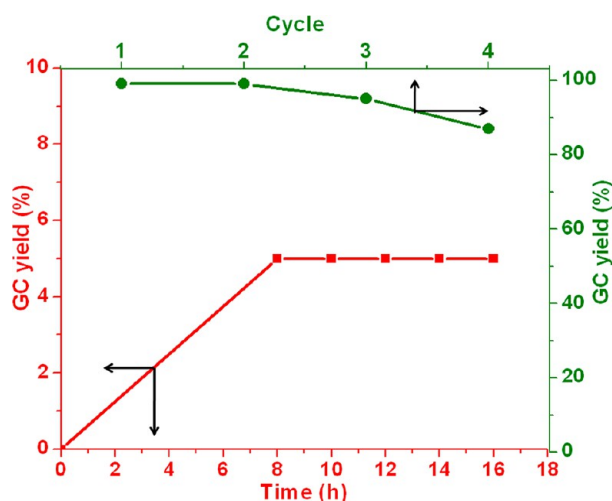


Figure 7. Heterogeneity and reusability tests of GNS-RuNPs.

[Figure S3 (ii) in Supporting Information]. The calculated Raman intensity ratio ( $I_D/I_G = 0.5143$ ) of *u*-GNPs-RuNPs was still high in comparison to *f*-GNS, which revealed that the RuNPs are still strongly attached to GNSs [Figure S3(iii) in Supporting Information]. XRD results confirmed that the chemical state of Ru was zero and was nanocrystalline in nature [Figure S3(iv) in Supporting Information]. Hence we conclude that GNS-RuNPs are physically as well as chemically stable and reusable.

**3.7. Effect of Particle Size on Catalytic Activity.** Owing to the high active surface area of MNPs, they are usually employed as a heterogeneous nanocatalyst in various reactions and facilitate better yields. Particularly, the MNPs having size of under 5 nm exhibited a dramatic catalytic activity.<sup>79</sup> Therefore, the effect of Ru particle size on catalytic efficiency in terms of yields has been investigated. For this purpose, another nanocatalyst with RuNP size of around 10–20 nm was prepared using the procedure pursued for the preparation of GNS-RuNPs; however, the mixing time was 5 min, and the calcination was carried out at 350 °C for 3 h. It is well known that MNPs can easily agglomerate to form bigger particles particularly at higher temperature due to their high specific surface energy.<sup>80</sup> Here, we postulate that the RuNPs might be agglomerated to form bigger RuNPs (10–20 nm) at the calcination temperature of 350 °C. The increase in the temperature from 300 to 350 °C increased the size of RuNPs from 1–3 nm to 10–20 nm; this suggests that the size of the RuNPs depends on the calcination temperature used. The TEM images [Figures 8(i) and (ii)] of this catalyst revealed that the RuNPs were well attached on the surface of the GNS with the particle size ranging from 10 to 20 nm. The mean diameter of RuNPs was found to be ca. 15 nm. The weight percentage of Ru was 4.34 in this catalyst [Figures 8(iii) and (iv)]. The calculated Raman intensity ratio ( $I_D/I_G$ ) was higher (0.2057) than that of the *f*-GNS; this indicates that the RuNPs were physically attached to the GNS surface [Figure 8(v)]. The XRD results confirmed that the RuNPs were in the zero oxidation state and had nanocrystalline nature [Figure 8(vi)]. The GNS-RuNP catalyst (10–20 nm) has a BET surface area of 35.1 m<sup>2</sup> g<sup>-1</sup> with a pore volume of 0.160 cm<sup>3</sup> g<sup>-1</sup> and a BJH desorption average pore diameter of 17 nm. The surface area per unit mass (*S*) of RuNPs was found to be 32.1 m<sup>2</sup> g<sup>-1</sup>. After the characterization, this nanocatalyst was employed in the

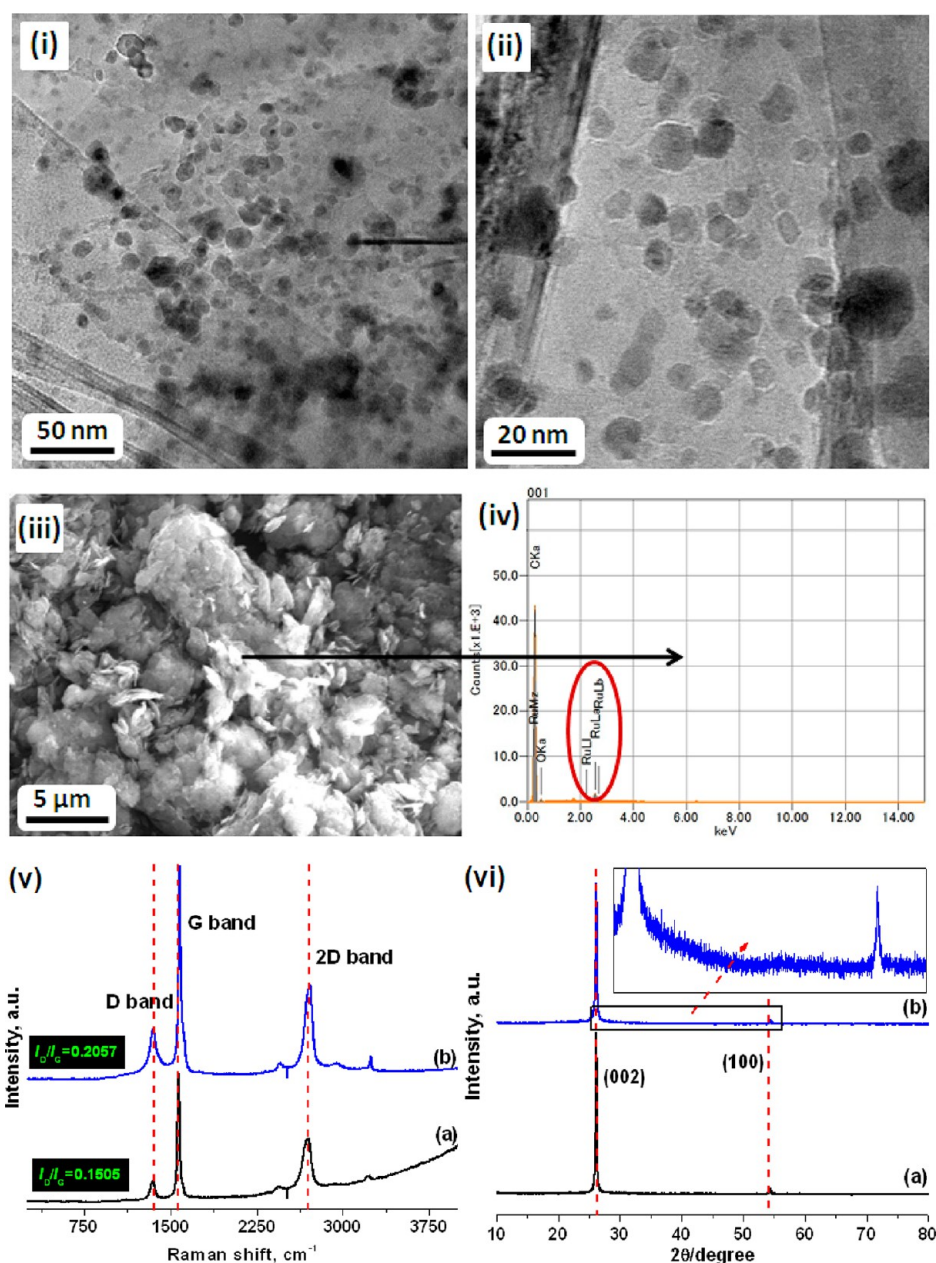
oxidation of alcohols, and efficiency was compared with GNS-RuNPs having 0.5–3 nm RuNPs (Table 3). As expected, the catalyst with 0.5–3 nm RuNPs exhibited a good catalytic activity in comparison to the one which contains RuNPs of 10–20 nm size. Hence, it is inferred that the excellent catalytic activity of GNS-RuNPs toward oxidation of alcohols is mainly due to the ultrafine structure of RuNPs (Table 3). Moreover, the activity of the catalyst in aerial oxidation reaction is obviously dependent on the size of RuNPs. In fact, when the size of RuNPs decreases, the surface area per unit mass (*S*) certainly increases. Consequently, a larger number of active sites are available. Thus, the GNS-RuNPs having Ru particle size of 0.5–3 nm showed excellent catalytic activity.<sup>81</sup> This argument is well supported by the BET surface area and the surface area per unit mass (*S*) of RuNPs.

**3.8. Proposed Mechanism.** To study the mechanism of GNS-RuNP catalyzed aerial oxidation of alcohols, FT-IR, Raman, and XPS spectra were recorded for GNS-RuNPs (pure nanocatalyst) and *o*-GNS-RuNPs (the nanocatalyst after stirring with 1-phenylethanol in 4 mL of toluene at 110 °C for 8 h); results are shown in Figure S4 in the Supporting Information. As expected, FT-IR spectra of GNS-RuNPs and *o*-GNS-RuNPs showed a peak at 1600 cm<sup>-1</sup> which was attributed to C=C stretching of GNSs. Interestingly, both FT-IR and Raman spectra of *o*-GNS-RuNPs showed a new peak at around 450 cm<sup>-1</sup>, which confirmed the formation of Ru-oxo species (Ru<sup>II</sup>=O) during the catalytic reaction.<sup>82</sup> In comparison to pure GNS-RuNPs, XPS spectra of *o*-GNS-RuNPs showed a positive shift in the O 1s peak with a dramatic increase in the peak intensity at 531.5 eV; this obviously confirmed the formation of Ru<sup>II</sup>=O during the oxidation reaction.<sup>82</sup> On the basis of the results obtained, we conclude that the mechanism for the oxidation of alcohols might be involving the Ru-oxo species as an intermediate (Figure 9). In the first step, RuNPs form Ru<sup>II</sup>=O species with the help of atmospheric oxygen. In the next step, the formed Ru-oxo species assisted the formation of acetophenone from 1-phenylethanol. Finally, the nanocatalyst was regenerated for the further oxidation process.

**3.9. Versatility of GNS-RuNPs.** The *u*-GNS-RuNPs were used to prepare ruthenium oxide nanorod hybrid GNS (*u*-GNS-RuO<sub>2</sub>NRs) which was characterized by TEM, SEM-EDS, XRD, Raman, and XPS. *u*-GNS-RuO<sub>2</sub>NRs were tested as a catalyst in the transfer hydrogenation of ketones.

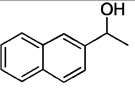
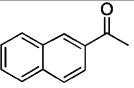
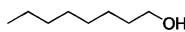
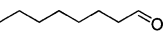
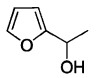
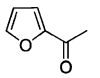
**3.9.1. Preparation and Characterization of *u*-GNS-RuO<sub>2</sub>NRs.** In a typical procedure, *u*-GNS-RuO<sub>2</sub>NRs were prepared by the calcination of *u*-GNS-RuNPs under a N<sub>2</sub> atmosphere at 600 °C for 6 h in a muffle furnace. The calcinated material was characterized and found to be *u*-GNS-RuO<sub>2</sub>NRs which were used as a catalyst for the transfer hydrogenation of ketones. The TEM images showed a very small and uniformly dispersed RuO<sub>2</sub>NR on GNSs [Figures 10(i) and (ii)]. The length and diameter of RuO<sub>2</sub>NRs were found in the range of 25–35 and 12–15 nm, respectively. The weight percentage of Ru in *u*-GNS-RuO<sub>2</sub>NRs was found to be 3.05 [Figure 10(iii)]. The elemental mapping of the *u*-GNS-RuO<sub>2</sub>NRs confirmed that the RuO<sub>2</sub>NRs were distributed uniformly on the surface of GNSs (Figure S5 in Supporting Information). The intensity ratio ( $I_D/I_G = 0.3162$ ) of *u*-GNPs-RuO<sub>2</sub>NRs was higher than that ( $I_D/I_G = 0.1505$ ) of *f*-GNSs, which revealed that the RuO<sub>2</sub>NRs were attached to the surface of GNSs. The BEs of Ru 3p<sub>3/2</sub> at 462.5 eV and Ru 3p<sub>1/2</sub> at 485.0 eV were attributed to the photoemission from RuO<sub>2</sub> (Ru<sup>4+</sup>) (Figure 10).<sup>84</sup> No X-ray diffraction peaks corresponding





**Figure 8.** (i and ii) TEM images and (iii and iv) SEM-EDS of GNS-RuNPs having 10–20 nm RuNPs, and (v) Raman and (vi) XRD spectra of GNS (a) and GNS-RuNPs having 10–20 nm RuNPs (b).

**Table 3.** Oxidation of Alcohols using GNS-RuNPs Having 10–20 nm RuNPs<sup>a</sup>

entry	substrate	product	t (h)	conv. <sup>b</sup> (%)	sel. <sup>b</sup> (%)	yield <sup>b</sup> (%)
1			18	54	100	54
2			20	39	100	39
3			22	10	100	10

<sup>a</sup>Reaction conditions: substrate (1 equiv), GNS-RuNPs having 10–20 nm RuNPs (0.036 mol %), toluene (4 mL), 110 °C. <sup>b</sup>Determined by GC analysis.

to RuO<sub>2</sub> were observed, which proved the nanocrystalline nature of RuO<sub>2</sub>NRs.<sup>85</sup>

**3.9.2. Transfer Hydrogenation of Ketones Catalyzed by *u*-GNS-RuO<sub>2</sub>NRs.** The *u*-GNS-RuO<sub>2</sub>NRs were investigated as

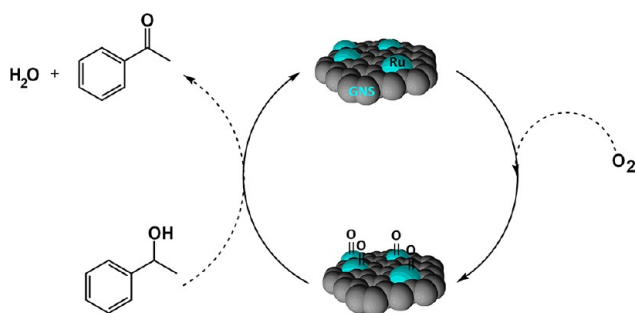


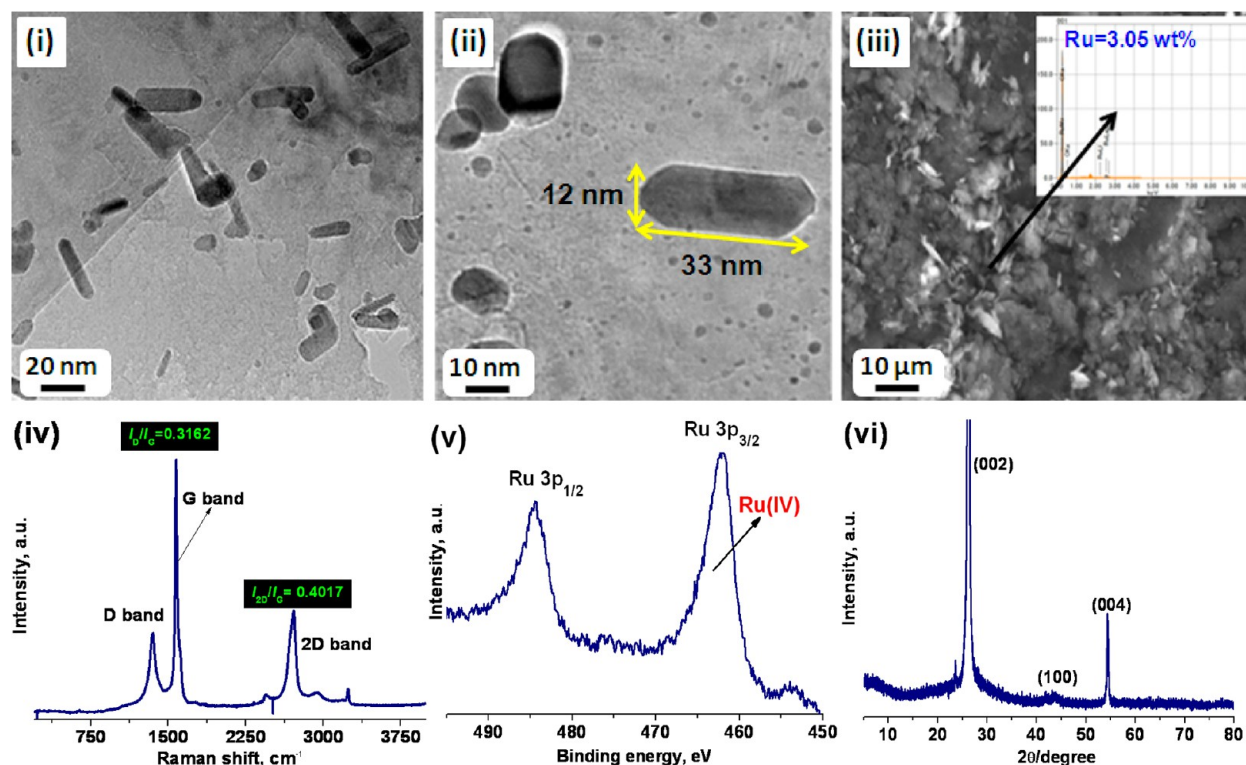
**Figure 9.** Proposed mechanism for GNS-RuNP catalyzed oxidation of alcohols.

catalyst for the transfer hydrogenation of ketones using 2-propanol as a hydrogen donor. Fortunately, acetophenone showed a very high conversion of 99% with 100% selectivity. Inspired by this result, the scope of the catalytic system was further extended to investigate a wide range of aromatic, alicyclic, and heterocyclic ketones (Table 4). The substituents have a moderate influence on the final yields, but the higher selectivity was maintained. 4-Bromoacetophenone was converted into its corresponding alcohol in 81% yield after stirring for 10 h (Table 4, entry 2). Hydrogenation of 4-methoxy benzophenone (Table 4, entry 3) proceeded with moderate yield of 62% (100% selectivity), which may be due to the presence of bulky substituent.<sup>86</sup> In the reduction of cycloheptanone to cycloheptanol, the present catalytic system showed a good yield of 88% with high selectivity of 100% (Table 4, entry 4), whereas HSi(OMe)-catalyzed reduction of cycloheptanone proceeded with the formation of the desired product in 76% yield.<sup>87</sup> Moreover, the present catalytic system can be adopted for the reduction of heterocyclic ketones as

well. It is noteworthy that 2-acetylthiophene was transformed to 1-thiophene ethanol (90%) with high selectivity, while silica-bound  $\text{RhCl}(\text{PPh}_3)_3$ -catalyzed reduction gave only 4% of the product.<sup>88</sup> Similarly, 1-furyl ethanone yielded 1-furyl ethanol in 76% yield, whereas  $\text{Pt}/\text{Al}_2\text{O}_3$ -catalyzed reaction yielded only 50% of the product.<sup>89</sup> The results concluded that the  $\mu$ -GNS-RuO<sub>2</sub>NRs effectively reduce various ketones; this confirms that the proposed catalyst (GNS-RuNPs) is highly stable and versatile.

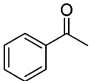
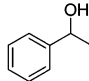
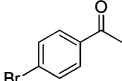
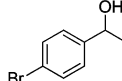
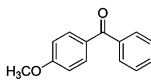
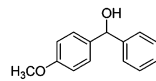
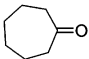
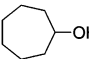
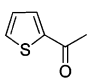
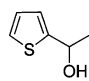
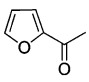
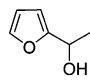
#### 4. CONCLUSIONS

In summary, we have successfully achieved bi- and few-layered GNSs from GNPs by a SPE method. The RuNPs were decorated on GNSs by a straightforward dry synthesis method, and TEM images confirmed good adhesion of RuNPs with a very narrow particle size distribution on GNSs. The weight percentage of Ru in GNS-RuNPs was 3.31, as determined by EDS analysis. Raman intensity ratios confirmed the attachment of RuNPs on the surface of GNSs. XRD and XPS revealed the metallic as well as nanocrystalline nature of RuNPs. The prepared GNS-RuNPs were able to oxidize effectively a wide range of alcohols into their corresponding carbonyl compounds in the presence of air. The nanocatalyst can also be used for selective oxidation of various aliphatic and aromatic alcohols. The amount of GNS-RuNP catalyst used for oxidation of alcohols was found to be as low as 5 mg (0.036 mol %), the lowest to the best of our knowledge. The ICP-MS result of the filtrate after the separation of the catalyst revealed the heterogeneous nature of the present catalysis. The excellent reusability of the GNS-RuNPs can be realized from the good yield of acetophenone (87%) from 1-phenylethanol even at the fourth run. The used GNS-RuNPs were transformed into  $\mu$ -GNS-RuO<sub>2</sub>NRs which showed good catalytic activity toward



**Figure 10.** (i and ii) TEM images, (iii) SEM-EDS, (iv) Raman, (v) XPS, and (vi) XRD of  $\mu$ -GNS-RuO<sub>2</sub>NRs.

Table 4. Transfer Hydrogenation of Ketones Catalyzed by  $\mu$ -GNPs-RuO<sub>2</sub>NRs<sup>a</sup>

$R_1-C(=O)-R_2 + CH_3CH(OH)CH_3 \xrightarrow[(CH_3)_3COK, 82^\circ C]{\mu\text{-GNPs-RuO}_2\text{NRs (0.033 mol\%)}} R_1-CH(OH)-R_2 + CH_3COCH_3$						
entry	substrate	product	t (h)	conv. <sup>b</sup> (%)	sel. <sup>b</sup> (%)	yield <sup>b</sup> (%)
1			12	99	100	99
2			10	81	100	81
3			16	62	100	62
4			24	88	100	88
5			20	95	95	90
6			20	92	84	76

<sup>a</sup>Reaction conditions: substrate (1 mmol),  $\mu$ -GNPs-RuO<sub>2</sub>NRs (0.033 mol %), (CH<sub>3</sub>)<sub>3</sub>COK (1 mmol), 2-propanol (4 mL), 82 °C. <sup>b</sup>Determined by GC analysis.

the transfer hydrogenation of various ketones. Overall, the simple synthesis, versatility, and good activity make GNS-RuNPs an alternate choice to the existing Ru-based catalysts.

## ■ ASSOCIATED CONTENT

### Supporting Information

Materials characterization, experimental procedures, and product analyses are available. This material is available free of charge via the Internet at <http://pubs.acs.org>.

## ■ AUTHOR INFORMATION

### Corresponding Authors

\*Phone: +81 268 21 5139. E-mail: [kim@shinshu-u.ac.jp](mailto:kim@shinshu-u.ac.jp).

\*Phone: + 91 431 2503636. E-mail: [kar@nitt.edu](mailto:kar@nitt.edu).

### Notes

The authors declare no competing financial interest.

## ■ ACKNOWLEDGMENTS

This work was supported by the grant-in-aid for global COE program by the Ministry of Education, Culture, Sports, Science, and Technology, Japan, and Department of Science and Technology, Ministry of Science and Technology, Government of India under FIST programme.

## ■ REFERENCES

- (1) Punniyamurthy, T.; Velusamy, S.; Iqbal, J. Recent Advances in Transition Metal Catalyzed Oxidation of Organic Substrates with Molecular Oxygen. *Chem. Rev.* **2005**, *105*, 2329–2364.
- (2) Lawrence, Q.; Tolman, W. B. Biologically Inspired Oxidation Catalysis. *Nature* **2008**, *455*, 333–340.
- (3) Arakawa, H. Catalysis Research of Relevance to Carbon Management: Progress, Challenges, and Opportunities. *Chem. Rev.* **2011**, *101*, 953–996.
- (4) Hill, C. L. *Advances in Oxygenated Processes*; Baumstark, A. L., Eds.; JAI: London, 1988.

(5) Hudlicky, M. *Oxidations in Organic Chemistry*; ACS Monograph Series; American Chemical Society: Washington, DC, 1990.

(6) Sheldon, R. A.; Kochi, J. K. *Metal Catalyzed Oxidations of Organic Compounds*; Academic Press: New York, 1981.

(7) Zhan, B. Z.; Thompson, A. Recent Developments in the Aerobic Oxidation of Alcohols. *Tetrahedron* **2004**, *60*, 2917–2935.

(8) Rhule, J. T.; Neiwert, W. A.; Hardcastle, K. I.; Do, B. T.; Hill, C. L. Ag<sub>5</sub>PV<sub>2</sub>Mo<sub>10</sub>O<sub>40</sub>: A Heterogeneous Catalyst for Air-Based Selective Oxidation at Ambient Temperature. *J. Am. Chem. Soc.* **2001**, *123*, 12101–12102.

(9) Choudary, B. M.; Kantam, M. L.; Rahman, A.; Reddy, C. V.; Rao, K. K. The First Example of Activation of Molecular Oxygen by Nickel in Ni-Al Hydrotalcite: A Novel Protocol for the Selective Oxidation of Alcohols. *Angew. Chem., Int. Ed.* **2001**, *40*, 763–766.

(10) Nishibayashi, Y.; Yamauchi, A.; Onodera, G.; Uemura, S. Oxidative Kinetic Resolution of Racemic Alcohols Catalyzed by Chiral Ferrocenyloxazolinylphosphine–Ruthenium Complexes. *J. Org. Chem.* **2003**, *68*, 5875–5880.

(11) Karimi, B.; Abedi, S.; Clark, J. H.; Budarin, V. Highly Efficient Aerobic Oxidation of Alcohols Using a Recoverable Catalyst: The Role of Mesoporous Channels of SBA-15 in Stabilizing Palladium Nanoparticles. *Angew. Chem., Int. Ed.* **2006**, *45*, 4776–4779.

(12) Oliveira, R. L.; Kiyohara, P. K.; Rossi, L. M. High Performance Magnetic Separation of Gold Nanoparticles for Catalytic Oxidation of Alcohols. *Green Chem.* **2010**, *12*, 144–149.

(13) Yamada, Y. M. A.; Arakawa, T.; Hocke, H.; Uozumi, Y. A Nanoplatinum Catalyst for Aerobic Oxidation of Alcohols in Water. *Angew. Chem., Int. Ed.* **2007**, *119*, 718–720.

(14) Mori, K.; Kanai, S.; Hara, T.; Mizugaki, T.; Ebitani, K.; Jitsukawa, K.; Kaneda, K. Development of Ruthenium–Hydroxyapatite-Encapsulated Superparamagnetic  $\gamma$ -Fe<sub>2</sub>O<sub>3</sub> Nanocrystallites as an Efficient Oxidation Catalyst by Molecular Oxygen. *Chem. Mater.* **2007**, *19*, 1249–1256.

(15) Tomioka, H.; Takai, K.; Nozaki, H.; Oshima, K. Selective Oxidation of a Primary Hydroxyl in the Presence of Secondary One. *Tetrahedron Lett.* **1981**, *22*, 1605–1608.

(16) Kanemoto, S.; Matsubara, S.; Takai, K.; Oshima, K. Transition-Metal Catalyzed Oxidation of Alcohols to Aldehydes and Ketones by means of Me<sub>3</sub>SiOOSiMe<sub>3</sub>. *Tetrahedron Lett.* **1983**, *24*, 2185–2188.



- (17) Backvall, J. E.; Chowdhury, R. L.; Karlsson, U. Ruthenium-Catalysed Aerobic Oxidation of Alcohols via Multistep Electron Transfer. *J. Chem. Soc., Chem. Commun.* **1991**, 473–475.
- (18) Pagliaro, M.; Campestrini, S.; Ciriminna, R. Ru-based Oxidation Catalysis. *Chem. Soc. Rev.* **2005**, 34, 837–845.
- (19) Bleloch, A.; Johnson, B. F. G.; Ley, S. V.; Price, A. J.; Shepard, D. S.; Thomas, A. W. Modified Mesoporous Silicate MCM-41 Materials: Immobilised Perruthenate – A New Highly Active Heterogeneous Oxidation Catalysts for Clean Organic Synthesis Using Molecular Oxygen. *Chem. Commun.* **1999**, 1999, 1907–1908.
- (20) Parmeggiani, C.; Cardona, F. Transition Metal Based Catalysts in the Aerobic Oxidation of Alcohols. *Green Chem.* **2012**, 14, 547–564.
- (21) Yamaguchi, K.; Mori, K.; Mizugaki, T.; Ebitani, K.; Kaneda, K. Creation of a Monomeric Ru Species on the Surface of Hydroxyapatite as an Efficient Heterogeneous Catalyst for Aerobic Alcohol Oxidation. *J. Am. Chem. Soc.* **2000**, 122, 7144–7145.
- (22) Yamaguchi, K.; Mizuno, N. Supported Ruthenium Catalyst for the Heterogeneous Oxidation of Alcohols with Molecular Oxygen. *Angew. Chem., Int. Ed.* **2002**, 41, 4538–4542.
- (23) Sheldon, R. A.; Arends, R. A.; Dijksman, A. New Developments in Catalytic Alcohol Oxidations for Fine Chemicals Synthesis. *Catal. Today* **2000**, 57, 157–166.
- (24) Yamaguchi, K.; Mizuno, N. Scope, Kinetics, and Mechanistic Aspects of Aerobic Oxidations Catalyzed by Ruthenium Supported on Alumina. *Chem.—Eur. J.* **2003**, 9, 4353–4361.
- (25) Matsumoto, M.; Ito, S. Ruthenium-Catalyzed Aerobic Oxidation of Pantoyl Lactone to Ketopantoyl Lactone. *Synth. Commun.* **1984**, 14, 697–700.
- (26) Murahashi, S. I.; Oda, Y.; Komiya, N.; Naota, T. Ruthenium-Catalyzed Oxidation of Alkanes with Peracids. *Tetrahedron Lett.* **1994**, 35, 7953–7956.
- (27) Choi, E.; Lee, C.; Na, Y.; Chang, S.  $[\text{RuCl}_2(\text{p-cymene})]_2$  on Carbon: An Efficient, Selective, Reusable, and Environmentally Versatile Heterogeneous Catalyst. *Org. Lett.* **2002**, 4, 2369–2371.
- (28) Komiya, N.; Nakae, T.; Sato, H.; Naota, T. Water-Soluble Diruthenium Complexes Bearing Acetate and Carbonate Bridges: Highly Efficient Catalysts for Aerobic Oxidation of Alcohols in Water. *Chem. Commun.* **2006**, 4829–4831.
- (29) Csajnyik, G.; Ell, A. H.; Fadini, L.; Pugin, B.; Backvall, J. E. Efficient Ruthenium-Catalyzed Aerobic Oxidation of Alcohols Using a Biomimetic Coupled Catalytic System. *J. Org. Chem.* **2002**, 67, 1657–1662.
- (30) Mori, S.; Takubo, M.; Makida, K.; Yanase, T.; Aoyagi, S.; Maegawa, T.; Monguchi, Y.; Sajiki, H. A Simple and Efficient Oxidation of Alcohols with Ruthenium on Carbon. *Chem. Commun.* **2009**, 5159–5161.
- (31) Yanga, X.; Wang, X.; Qiu, J. Aerobic Oxidation of Alcohols over Carbon Nanotube-Supported Ru Catalysts Assembled at the Interfaces of Emulsion Droplets. *Appl. Catal. A: Gen.* **2010**, 382, 131–137.
- (32) Geim, A. K.; Novoselov, K. S. The Rise of Graphene. *Nat. Mater.* **2007**, 6, 183–191.
- (33) Geim, A. K. Graphene: Status and Prospects. *Science* **2009**, 324, 1530–1534.
- (34) Stankovich, S.; Dikin, D. A.; Dommett, G. H. B.; Kohlhaas, K. M.; Zimney, E. J.; Stach, E. A.; Piner, R. D.; Nguyen, S. D.; Ruoff, R. S. Graphene-Based Composite Materials. *Nature* **2006**, 442, 282–286.
- (35) Machado, B. F.; Serp, P. Graphene-Based Materials for Catalysis. *Catal. Sci. Technol.* **2012**, 2, 54–75.
- (36) Schaezt, A.; Zeltner, M.; Stark, W. J. Carbon Modifications and Surfaces for Catalytic Organic Transformations. *ACS Catal.* **2012**, 2, 1267–1284.
- (37) Nethravathi, C.; Anumol, E. A.; Rajamathi, M.; Ravishankar, N. Highly Dispersed Ultrafine Pt and PtRu Nanoparticles on Graphene: Formation Mechanism and Electrocatalytic Activity. *Nanoscale* **2011**, 3, 569–571.
- (38) Gil, M. S.; Luigi, R.; Peter, S.; Willi, B.; Rolf, M. Palladium Nanoparticles on Graphite Oxide and its Functionalized Graphene Derivatives as Highly Active Catalysts for the Suzuki–Miyaura Coupling Reaction. *J. Am. Chem. Soc.* **2009**, 131, 8262–8270.
- (39) Kamat, P. V. Graphene-Based Nanoarchitectures. Anchoring Semiconductor and Metal Nanoparticles on a Two-Dimensional Carbon Support. *J. Phys. Chem. Lett.* **2010**, 1, 520–527.
- (40) Noyori, R.; Hashiguchi, S. Asymmetric Transfer Hydrogenation Catalyzed by Chiral Ruthenium Complexes. *Acc. Chem. Res.* **1997**, 30, 97–102.
- (41) Johnstone, R. A. W.; Wilby, A. H.; Entwistle, I. D. Heterogeneous Catalytic Transfer Hydrogenation and its Relation to other Methods for Reduction of Organic Compounds. *Chem. Rev.* **1985**, 85, 129–170.
- (42) Sanjib, B.; Lawrence, T. D. A Novel Approach to Create a Highly Ordered Monolayer Film of Graphene Nanosheets at the Liquid–Liquid Interface. *Nano Lett.* **2009**, 9, 167–172.
- (43) Xiaozhu, Z.; Xiao, H.; Xiaoying, Q.; Shixin, W.; Can, X.; Freddy, Y. C. B.; Qingyu, Y.; Peng, C.; Hua, Z. In Situ Synthesis of Metal Nanoparticles on Single-Layer Graphene Oxide and Reduced Graphene Oxide Surfaces. *J. Phys. Chem. C* **2009**, 113, 10842–10846.
- (44) Yang, J.; Tian, C.; Wang, L.; Fu, H. An Effective Strategy for Small-Sized and Highly-Dispersed Palladium Nanoparticles Supported on Graphene with Excellent Performance for Formic Acid Oxidation. *J. Mater. Chem.* **2011**, 21, 3384–3390.
- (45) Li, Y.; Fan, X.; Qi, J.; Ji, J.; Wang, S.; Zhang, G.; Zhang, F. Palladium Nanoparticle-Graphene Hybrids as Active Catalysts for the Suzuki Reaction. *Nano Res.* **2010**, 3, 429–437.
- (46) Li, J.; Liu, C. Y. Ag/Graphene Heterostructures: Synthesis, Characterization and Optical Properties. *Eur. J. Inorg. Chem.* **2010**, 2010, 1244–1248.
- (47) Tien, H. W.; Huang, Y. L.; Yang, S. Y.; Wang, J. Y.; Ma, C. C. M. The Production of Graphene Nanosheets Decorated with Silver Nanoparticles for use in Transparent, Conductive Films. *Carbon* **2011**, 49, 1550–1560.
- (48) Bai, S.; Shen, X. Graphene–Inorganic Nanocomposites. *RSC Adv.* **2012**, 2, 64–98.
- (49) Lin, Y.; Watson, K. A.; Fallbach, M. J.; Ghose, S.; Smith, J. G.; Delozier, D. M.; Cao, W.; Crooks, R. E.; Connell, J. W. Rapid, Solventless, Bulk Preparation of Metal Nanoparticle-Decorated Carbon Nanotubes. *ACS Nano* **2009**, 3, 871–884.
- (50) Hu, H.; Zhao, Z.; Zhou, Q.; Gogotsi, Y.; Qiu, J. The Role of Microwave Absorption on Formation of Graphene from Graphite Oxide. *Carbon* **2011**, 50, 3267–3273.
- (51) Yong, C. J.; Jin, H. K.; Takuya, H.; Yoong, A. K.; Morinobu, E.; Mauricio, T.; Mildred, S. D. Fabrication of Transparent, Tough, and Conductive Shape-Memory Polyurethane Films by Incorporating a Small Amount of High-Quality Graphene. *Macromol. Rapid Commun.* **2012**, 33, 628–634.
- (52) Lu, J.; Do, I.; Drzal, L. T.; Worden, R. M.; Lee, I. Nanometal-Decorated Exfoliated Graphite Nanoplatelet Based Glucose Biosensors with High Sensitivity and Fast Response. *ACS Nano* **2008**, 2, 1825–1832.
- (53) Liu, L. H.; Zorn, G.; Castner, D. G.; Solanki, R.; Lerner, M. M.; Yan, M. A Simple and Scalable Route to Wafer-Size Patterned Graphene. *J. Mater. Chem.* **2010**, 20, 5041–5046.
- (54) Zhou, X.; Huang, X.; Qi, X.; Wu, S.; Xue, C.; Boey, F. Y. C.; Yan, Q.; Chen, P.; Zhang, H. In Situ Synthesis of Metal Nanoparticles on Single-Layer Graphene Oxide and Reduced Graphene Oxide Surfaces. *J. Phys. Chem. C* **2009**, 113, 10842–10846.
- (55) Cancado, L. G.; Jorio, A.; Martins Ferreira, E. H.; Stavale, F.; Achete, C. A.; Capaz, R. B.; Moutinho, M. V. O.; Lombardo, A.; Kulmala, T. S.; Ferrari, A. C. Quantifying Defects in Graphene via Raman Spectroscopy at Different Excitation Energies. *Nano Lett.* **2011**, 11, 3190–3196.
- (56) Tjoa, V.; Jun, W.; Dravid, V.; Mhaisalkar, S.; Mathews, N. Hybrid Graphene–Metal Nanoparticle Systems: Electronic Properties and Gas Interaction. *J. Mater. Chem.* **2011**, 21, 15593–15599.
- (57) Dresselhaus, M. S.; Dresselhaus, G.; Saito, R.; Jorio, A. Raman Spectroscopy of Carbon Nanotubes. *Phys. Rep.* **2005**, 409, 47–99.

- (58) Sheng, Z. H.; Shao, L.; Chen, J. J.; Bao, W. J.; Wang, F. B.; Xia, X. H. Catalyst-Free Synthesis of Nitrogen-Doped Graphene via Thermal Annealing Graphite Oxide with Melamine and its Excellent Electrocatalysis. *ACS Nano* **2011**, *5*, 4350–4358.
- (59) North, J. M.; Van de Burgt, L. J.; Dalal, N. S. A Raman Study of the Single Molecule Magnet  $Mn_{12}$ -Acetate and Analogs. *Solid State Commun.* **2002**, *123*, 75–79.
- (60) Thomsen, C.; Reich, S. Double Resonant Raman Scattering in Graphite. *Phys. Rev. Lett.* **2000**, *85*, 5214–5217.
- (61) Michael, J. M.; Je-Luen, Li.; Douglas, H. A.; Hannes, C. S.; Ahmed, A. A.; Jun, L.; Margarita, H. A.; David, L. M.; Roberto, C.; Robert, K. P.; Ilhan, A. A. Single Sheet Functionalized Graphene by Oxidation and Thermal Expansion of Graphite. *Chem. Mater.* **2007**, *19*, 4396–4404.
- (62) Wei, T.; Fan, Z.; Zheng, C.; Yao, C.; Li, W. Movement-Induced Voltage Properties of Stable Graphite Nanoplatelet Suspensions. *Mater. Lett.* **2009**, *63*, 1608–1610.
- (63) Soldano, C.; Mahmood, A.; Dujardin, E. Production, Properties and Potential of Graphene. *Carbon* **2010**, *48*, 2127–2150.
- (64) Zhang, Y. B.; Small, J. P.; Pontius, W. V.; Kim, P. Fabrication and Electric-Field-Dependent Transport Measurements of Mesoscopic Graphite Devices. *Appl. Phys. Lett.* **2005**, *86*, 073104–073107.
- (65) Liu, C.; Kim, W. S.; Baek, J.; Cho, Y.; Han, S.; Kim, S. W.; Min, N. K.; Choie, Y.; Kim, J. U.; Lee, C. J. Improved Field Emission Properties of Double-walled Carbon Nanotubes Decorated with Ru Nanoparticles. *Carbon* **2009**, *47*, 1158–1164.
- (66) Akhavan, O. The Effect of Heat Treatment on Formation of Graphene Thin Films from Graphene Oxide Nanosheets. *Carbon* **2010**, *48*, 509–519.
- (67) Fan, X.; Peng, W.; Li, J.; Li, X.; Wang, S.; Zhang, G.; Zhang, F. Deoxygenation of Exfoliated Graphite Oxide under Alkaline Conditions: A Green Route to Graphene Preparation. *Adv. Mater.* **2008**, *20*, 4490–4493.
- (68) Kuila, T.; Bhadra, S.; Yao, D.; Kim, N. H.; Bose, S.; Lee, J. H. Recent Advances in Graphene Based Polymer Composites. *Prog. Polym. Sci.* **2010**, *35*, 1350–1375.
- (69) Chakroune, N.; Viau, G.; Ammar, S.; Poul, L.; Veautier, D.; Chehimi, M. M.; Mangeney, C.; Villain, F.; Fievet, F. Acetate- and Thiol-Capped Monodisperse Ruthenium Nanoparticles: XPS, XAS, and HRTEM Studies. *Langmuir* **2005**, *21*, 6788–6796.
- (70) Akhavan, O. Graphene Nanomesh by ZnO Nanorod Photocatalysts. *ACS Nano* **2010**, *4*, 4174–4180.
- (71) Kuila, T.; Bose, S.; Hong, C. E.; Uddin, M. E.; Khanra, P.; Kim, N. H.; Lee, J. H. Preparation of Functionalized Graphene/Linear Low Density Polyethylene Composites by a Solution Mixing Method. *Carbon* **2011**, *49*, 1033–1051.
- (72) Kerber, R. C. If it's Resonance, What is Resonating? *J. Chem. Educ.* **2006**, *83*, 223–227.
- (73) Zhao, M.; Li, J.; Song, Z.; Desmond, R.; Tschaen, D. M.; Grabowski, E. J. J.; Reider, P. J. A Novel Chromium Trioxide Catalyzed Oxidation of Primary Alcohols to the Carboxylic Acids. *Tetrahedron Lett.* **1998**, *39*, 5323–5326.
- (74) Hronec, M.; Cvengrosová, Z.; Kizlink, J. Competitive Oxidation of Alcohols in Aqueous Phase Using Pd/C Catalyst. *J. Mol. Catal.* **1993**, *83*, 75–82.
- (75) Yamaguchi, K.; Mizuno, N. Heterogeneously Catalyzed Liquid-Phase Oxidation of Alkanes and Alcohols with Molecular Oxygen. *New J. Chem.* **2002**, *26*, 972–974.
- (76) Velusamy, S.; Punniyamurthy, T. Novel Vanadium-Catalyzed Oxidation of Alcohols to Aldehydes and Ketones under Atmospheric Oxygen. *Org. Lett.* **2004**, *6*, 217–219.
- (77) Su, F. Z.; Liu, Y. M.; Wang, L. C.; Cao, Y.; He, H. Y.; Fan, K. N. Ga–Al Mixed-Oxide-Supported Gold Nanoparticles with Enhanced Activity for Aerobic Alcohol Oxidation. *Angew. Chem., Int. Ed.* **2008**, *120*, 340–343.
- (78) Oliveira, R. L.; Kiyohara, P. K.; Rossi, L. M. High Performance Magnetic Separation of Gold Nanoparticles for Catalytic Oxidation of Alcohols. *Green Chem.* **2010**, *12*, 144–149.
- (79) Joo, S. H.; Park, J. Y.; Renzas, J. R.; Butcher, D. R.; Huang, W.; Somorjai, G. A. Size Effect of Ruthenium Nanoparticles in Catalytic Carbon Monoxide Oxidation. *Nano Lett.* **2010**, *10*, 2709–2713.
- (80) Arvela, P. M.; Murzin, D. Y. Effect of Catalyst Synthesis Parameters on the Metal Particle Size. *Appl. Catal. A: Gen.* **2013**, *451*, 251–281.
- (81) Bell, A. T. The Impact of Nanoscience on Heterogeneous Catalysis. *Science* **2003**, *299*, 1688–1691.
- (82) Hirai, Y.; Kojima, T.; Mizutani, Y.; Shiota, Y.; Yoshizawa, K.; Fukuzumi, S. Ruthenium-Catalyzed Selective and Efficient Oxygenation of Hydrocarbons with Water as an Oxygen Source. *Angew. Chem., Int. Ed.* **2008**, *120*, 5856–5860.
- (83) Rochefort, D.; Dabo, P.; Guay, D.; Sherwood, P. M. A. XPS Investigations of Thermally Prepared  $RuO_2$  Electrodes in Reductive Conditions. *Electrochim. Acta* **2003**, *48*, 4245–4252.
- (84) Sankar, J.; Sham, T. K.; Puddephatt, R. J. Low Temperature Chemical Vapour Deposition of Ruthenium and Ruthenium Dioxide on Polymer Surfaces. *J. Mater. Chem.* **1999**, *9*, 2439–2444.
- (85) Mirosław, Z.; Janina, O. Synthesis and Structure Characterization of Ru Nanoparticles Stabilized by PVP or  $\gamma-Al_2O_3$ . *Mater. Res. Bull.* **2008**, *43*, 3111–3121.
- (86) Noyori, R.; Ohkuma, T. Asymmetric Catalysis by Architectural and Functional Molecular Engineering: Practical Chemo- and Stereoselective Hydrogenation of Ketones. *Angew. Chem., Int. Ed.* **2001**, *40*, 40–73.
- (87) Hosomi, A.; Hayashida, H.; Kohra, S.; Tominaga, Y. J. Penta Coordinate Silicon Compounds in Synthesis: Chemo- and Stereoselective Reduction of Carbonyl Compounds Using Trialkoxy-Substituted Silanes and Alkali Metal Alkoxides. *J. Chem. Soc., Chem. Commun.* **1986**, *1986*, 1411–1412.
- (88) Bogar, K.; Krumlinde, P.; Bacsik, Z.; Hedin, N.; Backvall, J. E.; Ruiz, J. R.; Sanchidrian, C. J.; Hidalgo, J. M.; Marinas, J. M. Heterogenized Wilkinson-Type Catalyst for Transfer Hydrogenation of Carbonyl Compounds. *Eur. J. Org. Chem.* **2011**, *2011*, 4409–4414.
- (89) Kijenski, J.; Winiarek, P.; Paryczak, T.; Lewicki, A.; Mikołajska, A. Platinum Deposited on Monolayer Supports in Selective Hydrogenation of Furfural to Furfuryl Alcohol. *Appl. Catal. A: Gen.* **2002**, *233*, 171–182.